

NMR study of spin excitations in carbon nanotubes

P. M. Singer¹, P. Wzietek¹, H. Alloul^{*1}, F. Simon², and H. Kuzmany²

¹ Laboratoire de Physique des Solides, UMR 8502, Université Paris-Sud, 91405 Orsay, France

² Institut für Materialphysik, Universität Wien, Strudlhofgasse 4, 1090 Wien, Austria

Received 14 June 2006, accepted 15 September 2006

Published online 11 October 2006

PACS 61.46.+w, 71.20.Tx, 73.22.-f, 76.60.-k

The spin dynamics of ¹³C isotope enriched inner-walls in double-wall carbon nanotubes (DWCNT) has been studied using ¹³C nuclear magnetic resonance (NMR). Contrary to expectations, the spin–lattice relaxation time (T_1) has the same temperature (T) and magnetic field (H) dependence for most of the inner-wall nanotubes detected by NMR. In the high temperature regime ($T \gtrsim 150$ K), we find that the T and H dependence of $1/T_1T$ is consistent with a 1D metallic chain. For $T \lesssim 150$ K the data clearly indicates the formation of a gap in the spin excitation spectrum, where the gap value $2\Delta = 40$ K ($\equiv 3.7$ meV) is H independent.

© 2006 WILEY-VCH Verlag GmbH & Co. KGaA, Weinheim

The electronic properties of carbon nanotubes have been a topic of intense investigation ever since their discovery in early 1990's. According to band-structure calculations the basic electronic structure of single-wall carbon nanotubes (SWCNT) is expected to depend on the chiral wrapping vector (n, m) across the graphene plane, where tubes for which $(2n + m)/3 = \text{integer}$ are metallic, while all other tubes are semiconducting [1–4] with a large ~ 1 eV gap [5]. While STM and transport measurements on *isolated* tubes demonstrate the diversity of tube properties, significant measurements on *macroscopic* amounts of tubes are only possible in selected cases. Recently, double wall carbon nanotubes (DWCNT) have been synthesized by filling SWCNT with fullerenes (so called “peapods”[6]) followed by a high temperature reaction [7, 8]. These DWCNT have some exceptional properties since the inner tubes are accommodated in a highly shielded environment under clean room conditions [9].

Nuclear magnetic resonance (NMR) is usually an excellent technique for probing the electronic properties at the Fermi level of metallic systems, however, the 1.1% natural abundance of ¹³C limits the sensitivity of such experiments. Data taken on SWCNT essentially evidence a large distribution of properties since samples of identical tubes are presently out of reach. Here, selective enrichment of the inner shells using ¹³C isotope enriched fullerenes [10, 11] in the peapod synthesis route was used to probe the specific properties of the inner tubes. The ¹³C enrichment increases the NMR sensitivity but also allows us to achieve *selective* enrichment of the inner shells alone. This provides us with the possibility of singling out the electronic properties of these inner tubes for the first time [12]. We show that, although these tubes are distributed in diameter and chirality, their electronic properties display a strikingly homogeneous behavior.

Macroscopic information about enrichment can be obtained from NMR spectroscopy as it measures the number of ¹³C [10]. In Fig. 1 we show the static and MAS spectra of ¹³C enriched DWCNTs as well as the static spectrum of the SWCNT starting material. The mass fraction belonging to the enriched phase relative to the total sample mass can be calculated from the integrated NMR signal by comparing it to the NMR signal of the 89% ¹³C enriched fullerene, we found this fraction to be 13%. The expected

* Corresponding author: e-mail: alloul@lps.u-psud.fr

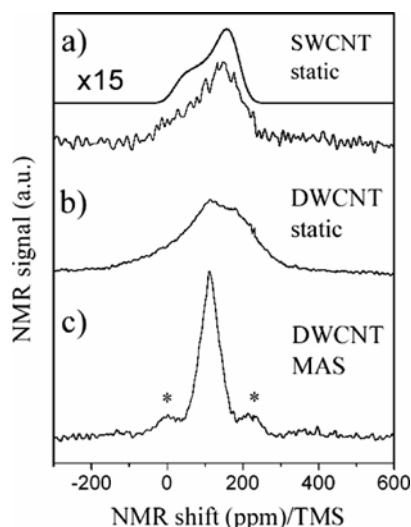


Fig. 1 NMR spectra normalized by the sample mass: (a) static spectrum for non enriched SWCNT enlarged by a factor of 15, (b) static and (c) MAS spectra of $^{13}\text{C}_{0.89}$ -DWCNT. Smooth curve is a simulated CSA powder pattern. Spinning sidebands at 8 kHz are marked with asterisks. Frequency reference is TMS line.

mass ratio of inner tubes as compared to the total sample mass is 15%, which is obtained from the SWCNT purity (50%), $\approx 70\%$ volume filling in highly filled peapod samples, and the mass ratio of encapsulated fullerenes to the mass of the SWCNTs. The measured mass fraction of the highly enriched phase is very similar to that of the calculated fraction of inner tubes. This suggests that the NMR signal comes nominally from inner tubes and that other carbon phases such as amorphous or graphitic carbon are not enriched.

We probed the low frequency spin dynamics (or low energy spin excitations, equivalently) of the inner-tubes using the spin–lattice relaxation time, T_1 , defined as the characteristic time it takes the ^{13}C nuclear magnetization to recover after saturation. The signal intensity after saturation, $S(t)$, was deduced by integrating the fast Fourier transform of half the spin-echo for different delay times t . We obtained the value of T_1 by fitting the t dependence of $S(t)$ to the form $S(t) = S_a - S_b \cdot M(t)$, where $S_a \approx S_b$ (> 0) are arbitrary signal amplitudes, and

$$M(t) = \exp\left[-(t/T_1^e)^\beta\right], \quad (1)$$

is the reduced magnetization recovery of the ^{13}C nuclear spins. Figure 2 shows the results of $M(t)$ for the inner-tubes as a function of the scaled delay time t/T_1^e , under various experimental conditions listed in the figure. We find that $M(t)$ does not follow the single exponential form with $\beta = 1$ (dashed line), but instead fits well to the stretched exponential form with $\beta \approx 0.65(5)$ which implies a distribution in underlying relaxation times T_1 across the sample. In such cases, T_1^e in Eq. (1) is directly proportional to the mean value \bar{T}_1 of the T_1 distribution as such $T_1^e = \bar{T}_1 \cdot \beta/\Gamma(1/\beta)$, where Γ is the gamma function. We display the data in Fig. 2 on a semi-log scale for the *time* axis in order to accentuate the data for earlier decay times and to illustrate the collapse of the data set for the upper 90% of the NMR signal. We find that the upper 90% of the $M(t)$ data is consistent with constant $\beta \approx 0.65(5)$, implying a constant underlying distribution in T_1 for a large range of experimental conditions. The lower 10% of the $M(t)$ data (corresponding to longer delay times) comes from the non-enriched outer-walls which, as a result of their larger diameters, have much longer relaxation times under similar experimental conditions [14–17].

Two distinct origins for the multi-exponential magnetization recovery can be considered. The first is due to the powder average over the spatial anisotropy in T_1 . The distribution is independent of the tube properties, and can also be found in the ^{13}C NMR data for alkali doped fullerenes A_nC_{60} [18, 19]. Given the similar diameter of C_{60} ($d = 0.71$ nm) to the average inner-wall diameter ($\bar{d} = 0.7$ nm [10, 11]) in this report, we can expect comparable bonding effects for the electron orbitals. It has been shown that in A_nC_{60} the T_1 for ^{13}C is dominated by dipole–dipole interactions between the electron spin in the $p\pi$

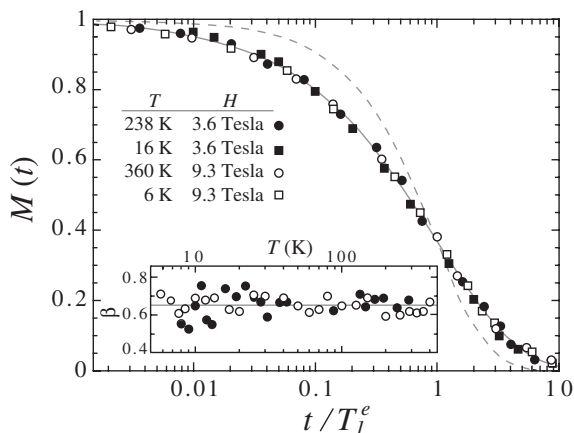


Fig. 2 Reduced nuclear magnetization recovery, $M(t)$, as a function of the scaled delay time t/T_1^e (see Eq. (1)), for various experimental conditions. Both axes are dimensionless. Solid grey curve shows stretched exponential fit with $\beta = 0.65$, while grey dashed curve shows single exponential with $\beta = 1$. *inset*: Temperature dependence of the best fit values of β at 3.6 Tesla (\bullet) and 9.3 Tesla (\circ), and average value of the data set $\beta = 0.65$ (solid line).

bond and the ^{13}C nuclear spin [20]. In this case, the relaxation depends on the orientation of the p_π orbital (which is perpendicular to the tube surface) and the external magnetic field, and therefore contributes to the multi-exponential form of magnetization recovery for a powder average. This resultant T_1 distribution is independent of T and H .

Another source of multi-exponential recovery is from a distribution of the inner tube properties themselves, such as their diameter. According to Raman scattering, the inner tubes have a mean diameter of $\bar{d} \approx 0.7$ nm with a standard deviation of $\sigma \approx 0.1$ nm [10, 11]. Within this distribution lies a variety of tubes with different chirality and one can *a priori* expect to find metallic as well as semiconducting tubes [3]. If both semiconducting and metallic inner-tubes existed in our sample, one would expect the ratio of the T_1 's between the different tubes to increase exponentially with decreasing T below the semiconducting gap (~ 5000 K [5]), which would drastically change the underlying T_1 distribution with decreasing T . This change would manifest itself as a large change in the shape of the recovery $M(t)$, however, as shown in Fig. 2 this is *not* the case. We can therefore rule out the possibility of two components in T_1 with different T dependences, and instead we conclude *that all T_1 components exhibit the same T and H dependence within experimental scattering*.

The T_1 distribution in the sample, whether it arises from anisotropy or diameter variations (or both), shows a uniform T and H dependence. It is therefore appropriate to follow the T and H dependence of the mean value of the distribution (T_1^e in Eq. (1)), and thereby get insight into the homogenous electronic state of the inner tubes. In order to avoid unnecessary experimental scattering in T_1^e , we then go back and fit all the $M(t)$ data to Eq. (1) with a *fixed* value of $\beta = 0.65$. We plot the resulting temperature dependence of $1/T_1^e T$ in Fig. 3(*left*) for two different values of the magnetic field H . We can immediately separate the data into two temperature regimes: the high temperature regime $\gtrsim 150$ K, and the low T regime $\lesssim 150$ K. At high temperatures we find that $1/T_1^e T$ is independent of T which indicates a metallic state [13], which given the arguments above implies that all of the inner tubes are metallic. We also observe a strong field dependence for T_1 . As was shown in [12], for H values ranging from 1.2 Tesla to 9.3 Tesla the data fit well to the form $1/T_1^e T = A + B/\sqrt{H}$, where A and B are constants. This is very suggestive of a 1D spin diffusion mechanism for T_1 where B/\sqrt{H} corresponds to the diffusive contribution to the relaxation originating from the long wavelength (i.e. $q \approx 0$) modes while A corresponds to the non-diffusive contributions from $q > 0$ modes. Therefore the high-temperature regime is consistent with a 1D metallic chain picture.

The origin of the unusual T dependence of $1/T_1^e T$ in the low temperature regime ($\lesssim 150$ K) is not immediately obvious. We can however rule out certain possibilities. Firstly, we can rule out the possibility of an activation type mechanism where T_1 is dominated by fluctuating hyperfine fields which are slowing down with decreasing T . If this were the case the temperature where $1/T_1^e T$ reached its maxi-

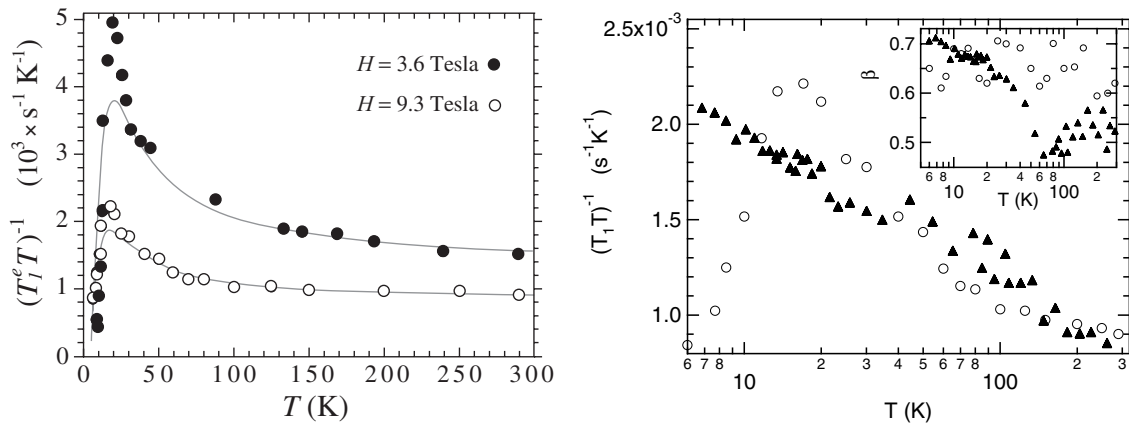


Fig. 3 *Left:* Temperature dependence of spin–lattice relaxation rate divided by temperature, $1/T_1^e T$. Grey curves are best fits to the model with $2\Delta = 46.8(40.2)$ K for $H = 3.6(9.3)$ Tesla, respectively. *Right:* Comparison of temperature dependencies of $1/T_1^e T$ and β for sealed (circles) and oxygen-exposed samples (triangles) at $H = 9.3$ Tesla.

mum would shift with the resonance frequency ω [13], i.e. with the applied magnetic field. As shown in Fig. 3, however, we find no evidence of a shift in the peak temperature with H . Furthermore, at low temperatures $1/T_1^e T$ is found to drop below its high temperature value which rules out the possibility of an activation contribution *plus* a T independent contribution. Secondly, we also rule out the possibility of relaxation by paramagnetic centers which can arise from wall defects or impurity spins. The behavior of $1/T_1^e T$ implies a pronounced *gap* in the low energy spin excitation spectrum, which cannot be explained by the presence of paramagnetic centers.

Having ruled out the above possibilities, we are then lead to consider the simplest explanation for the experimental data using a non-interacting electron model of a 1D semiconductor with a small secondary gap (SG). The SG may be a result of the finite inner-wall curvature [4, 5, 21, 22], or perhaps the applied magnetic field itself [23]. Taking the normalized form of density-of-states $n(E)$

$$n(E) = \begin{cases} \frac{E}{\sqrt{E^2 - \Delta^2}} & \text{for } |E| > \Delta \\ 0 & \text{otherwise} \end{cases} \quad (2)$$

we can easily calculate $1/T_1^e T$ for a 1D electron band [12]. The model has only one free parameter, the homogeneous SG, 2Δ . The results of the best fit (obtained by numerical calculation) are presented in Fig. 3, where $2\Delta = 43(3)$ K ($\equiv 3.7$ meV). At high temperature, when $T \gg 2\Delta$, the gap is irrelevant and we recover the usual Korringa law $1/T_1^e T = \text{const}$ for metals [13], however when T approaches the gap there is an increase of $1/T_1^e T$ due to the van-Hove singularity in the density of states (Eq. (2)). The gap is found to be H independent (within experimental scattering) between 9.3 and 3.6 Tesla.

What could possibly be the origin of the observed gap? Tight binding calculations predict that applied magnetic fields can induce SG's of similar magnitude for metallic SWCNT [23]. However, such a scenario is excluded here from the absence of field dependence of the observed gap. Our data would be more consistent with a curvature induced SG for metallic tubes [4, 5, 21, 22], however for our typical inner-tubes the predicted values, ~ 100 meV, are over an order of magnitude larger than our experimental data. Other scenarios, such as quantization of levels due to finite short lengths of the nanotubes could be considered as well, however, in all these cases a behavior independent of tube size and chirality is certainly not expected.

This leads us to consider the effect of electron–electron interactions for the metallic inner tubes. Photoemission spectroscopy (PES) measurements on metallic tubes in bundles [25, 26] suggest indeed

that strong electron–electron correlations can lead to a Tomonaga–Luttinger-liquid (TLL) state. It has been predicted that a TLL state should lead to an observable increase in $1/T_1T$ with decreasing T [24]. The correlated 1D nature may also lead to a Peierls instability [3] with the opening of a small collective gap 2Δ and a sharp drop in $1/T_1T$ below $\Delta \sim 20$ K. Therefore, the presence of both a TLL state *and* a Peierls instability could possibly account for the data, although here again, the independence on tube geometry should be accounted for.

All ^{13}C NMR data shown above were taken with the sample sealed in a glass tube filled with 200 mbar of high purity Helium gas. In Fig. 3 (*right*) we compare the relaxation curve of Fig. 3 (*left*) with the one obtained in the same conditions for a similar sample exposed to oxygen atmosphere (200 mbar Helium + 200 mbar O_2). It is seen that the gap feature has disappeared and the relaxation profile has acquired a paramagnetic-like component which persists down to the lowest temperatures. Oxygen can be embedded in nanotube channels as well as bind to defects in the nanotube structure. At this time it is not clear what is its effect on the inner-wall nanotube DOS, however, since $1/T_1T$ is about the same at high T for both samples, it is more likely to induce impurity magnetism which dominates the relaxation at low T then to merely suppress the gap.

In conclusion, we have shown that the electronic properties of the inner wall nanotubes behave as for a 1D metal at room T , but exhibit a pronounced gap below ≈ 20 K. The T_1 recovery data indicate that most of the inner-tubes have similar T and H dependences, with no indication of a metallic/semiconductor separation due to chirality distributions. The metallicity at high temperatures might result from charge transfer from the outer to the inner tubes, however this speculation ought to be confirmed by independent experiments and theoretical calculations. We list various interpretations for the gapped behavior at low T , ranging from a non-interacting secondary band-gap model to a 1D correlated electron model with a collective gap (possibly a Peierls instability). Our unexpected results reveal that such a macroscopic collection of carbon nanotubes is an object displaying original physical properties worth studying in more detail with macroscopic experimental techniques. These results also appeal for further experimental investigations on diversely synthesized DWCNT in order to check whether these observations are specific to the “peapod” synthesis route. Theoretical work on the incidence of 1D correlation effects for inner-wall nanotubes inside DWCNT should be helpful in sorting out the origin of our astonishing experimental evidence.

Acknowledgements Support from the EU projects HPMF-CT-2002-02124, HPRN-CT-2002-00192, and MERG-CT-2005-022103, and the Austrian Science Funds (FWF) project Nr. 17345, are recognized. The authors also wish to thank V. Zólyomi and J. Kürti for valuable discussions. F.S. acknowledges the Zoltán Magyary programme and the Hungarian State Grants (OTKA) Nr. TS049881, F61733 and NK60984.

References

- [1] J. W. Mintmire et al., Phys. Rev. Lett. **68**, 631 (1992).
- [2] R. Saito et al., Phys. Rev. B **46**, 1804 (1992).
- [3] R. Saito, G. Dresselhaus, and M. Dresselhaus, Physical Properties of Carbon Nanotubes (Imperial College Press, London, 1998).
- [4] N. Hamada et al., Phys. Rev. Lett. **68**, 1579 (1992).
- [5] J. W. Mintmire and C. T. White, Phys. Rev. Lett. **81**, 2506 (1998).
- [6] B. W. Smith et al., Nature (London) **396**, 323 (1998).
- [7] B. W. Smith and D. E. Luzzi, Chem. Phys. Lett. **321**, 169 (1999).
- [8] S. Bandow et al., Chem. Phys. Lett. **384**, 320 (2004).
- [9] R. Pfeiffer et al., Phys. Rev. Lett. **90**, 225501 (2003).
- [10] F. Simon et al., Phys. Rev. Lett. **95**, 17401 (2005).
- [11] F. Simon et al., Phys. Rev. B **71**, 165439 (2005).
- [12] P. M. Singer et al., Phys. Rev. Lett. **95**, 236403 (2005).
- [13] C. P. Slichter, Principles of Magnetic Resonance, 3rd ed. (Springer-Verlag, New York, 1989).
- [14] X.-P. Tang et al., Science **288**, 492 (2000).

- [15] C. Goze-Bac et al., *Carbon* **40**, 1825 (2002).
- [16] H. Shimoda et al., *Phys. Rev. Lett.* **88**, 15502 (2002).
- [17] A. Kleinhammes et al., *Phys. Rev. B* **68**, 75418 (2003).
- [18] R. Tycko et al., *Phys. Rev. Lett.* **68**, 1912 (1992).
- [19] V. Brouet et al., *Phys. Rev. B* **66**, 155122 (2002).
- [20] V. Antropov et al., *Phys. Rev. B* **47**, R12373 (1993).
- [21] C. L. Kane and E. J. Mele, *Phys. Rev. Lett.* **78**, 1932 (1997).
- [22] V. Zolyomi and J. K rti, *Phys. Rev. B* **70**, 85403 (2004).
- [23] J. P. Lu, *Phys. Rev. Lett.* **74**, 1123 (1995).
- [24] H. Yoshioka, *J. Phys. Chem. Solids* **63**, 1281 (2002).
- [25] H. Ishii et al., *Nature* **426**, 540 (2003).
- [26] H. Rauf et al., *Phys. Rev. Lett.* **93**, 96805 (2004).